frontiers | Frontiers in Environmental Science

TYPE Methods
PUBLISHED 28 November 2022
DOI 10.3389/fenvs.2022.1054076

OPEN ACCESS

EDITED BY
Dongmei Xu,
Nanjing University of Information Science and Technology, China

REVIEWED BY
Yinan Li,
China Academy of Space Technology (CAST), China
Mukesh Gupta,
Independent Researcher, Calgary, AB, Canada

*CORRESPONDENCE
Weihua Ai,
awhzjax@126.com

SPECIALTY SECTION
This article was submitted to Environmental Informatics and Remote Sensing, a section of the journal Frontiers in Environmental Science

RECEIVED 26 September 2022
ACCEPTED 03 November 2022
PUBLISHED 28 November 2022

CITATION
Guo C, Ai W, Liu M, Feng M, Qiao J and Hu S (2022), Sea surface temperature retrieval based on simulated space-borne one-dimensional multifrequency synthetic aperture microwave radiometry.
Front. Environ. Sci. 10:1054076.
doi: 10.3389/fenvs.2022.1054076

Sea surface temperature retrieval based on simulated space-borne one-dimensional multifrequency synthetic aperture microwave radiometry

Chaogang Guo, Weihua Ai*, Maohong Liu, Mengyan Feng, Junqi Qiao and Shensen Hu

College of Meteorology and Oceanography, National University of Defense Technology, Changsha, China

The space-borne one-dimensional multifrequency synthetic aperture microwave radiometer (1D-MSAMR) offers new possibilities for detecting high spatial resolution sea surface temperature (SST). To achieve higher SST retrieval accuracy, an SST retrieval algorithm, the two-step retrieval algorithm (TSSR), is proposed based on the multiple linear regression (MLR) algorithm. In this study, we investigated the SST retrieval accuracy of 1D-MSAMR based on simulation experiments. For the study, we assumed that the frequencies of the 1D-MSAMR were 6.9, 10.65, 18.7, 23.8, and 36.5 GHz, and that all frequencies worked in a dual polarization (vertical and horizontal) manner. We used an ocean-atmosphere microwave radiation brightness temperature model and the 1D-MSAMR simulator to simulate the measured brightness temperature based on WindSat data provided by the Remote Sensing Systems (RSS). An MLR algorithm and the TSSR were then developed to retrieve the SST within the incidence angle range of 0°–65°. The results show that the SST retrieval errors of the two SST retrieval algorithms decreased with the increase of incidence angle. The TSSR had higher retrieval accuracy, especially at low incidence angle. The average retrieval accuracy of the TSSR was about 0.3 K higher than that of the MLR algorithm. The retrieval error of the TSSR was also less sensitive to the measurement error of the 6.9 GHz frequency than the MLR algorithm.

KEYWORDS

space-borne one-dimensional multifrequency synthetic aperture microwave radiometer, sea surface temperature retrieval, two-step retrieval algorithm, multiple incidence angles, frequency

1 Introduction

With the development of satellite remote sensing technologies, remote sensing data is now being used to monitor global sea surface temperature (SST). Clouds and aerosols are essentially transparent to microwave radiation at frequencies below about 12 GHz, therefore microwave remote sensing can potentially eliminate the atmospheric

contamination problems that plague infrared measurements and is considered an enabling technology for all-day and all-weather SST measurement (Chelton and Wentz, 2005). Most microwave radiometers in orbit are real-aperture radiometers with conical scanning, such as the TMI, WindSat, AMSR2, and HY-2. Real-aperture microwave radiometers require large and massive antennas for high spatial resolution, such as that of the CIMR (Ulaby, 1981; Lise et al., 2018).

A synthetic aperture microwave radiometer using an interferometric technique is proposed to overcome the barriers that antenna size has placed on passive microwave sensing from space (RYLE, 1962; Vine, 2000). In such systems, the correlation of the output voltage from pairs of antennas with different spacing (baselines) is measured (Le et al., 1994; Jin et al., 2019). The product at each baseline yields a sample point in the Fourier transform of the brightness temperature map of the scene, and the scene itself is reconstructed by inverting the sampled transform (Le and David, 1990; Vine et al., 1992).

Several synthetic aperture microwave radiometers have been developed for Earth observation, such as electronically steered thinned array L-band radiometer (ESTAR) (Vine et al., 2004), MIRAS (Zine et al., 2008), and GeoSTAR (Lambrigtsen et al., 2006). The first space-borne synthetic aperture microwave radiometer, MIRAS, was mounted onboard the SMOS (Soil Moisture and Ocean Salinity) satellite which is a Y-sparse structure having many small receivers evenly distributed along the arms (Zine et al., 2008). The MIRAS provides soil moisture and ocean surface salinity global coverage measurements from space (Jordi et al., 2010). A study called MICROWAT showed that two-dimensional interferometric systems would be very complex (with a 3.9 K sensitivity on each measurement) and would not satisfy the user requirements in terms of SST accuracy. As a practical alternative, a one-dimensional interferometric system has a much lower systematic complexity, with 0.15 K sensitivity at 6.9 GHz and 0.35 K sensitivity at 18.7 GHz (Prigent et al., 2013).

The first one-dimensional synthetic aperture microwave radiometer (1D-MSAMR), ESTAR, was installed on an aircraft and operates at L-band. This system adopts the real-aperture along the track and the synthetic aperture cross-track dimension, and obtains an angular resolution of 7° (Le et al., 1994). The HUST-ASR is a one-dimensional synthetic aperture microwave radiometer developed by Huazhong University of Science and Technology that generates high-quality images of natural scenes (Li et al., 2008). An SST sensitivity and physical retrieval method based on the C-band 1D-MSAMR has been investigated (Ai et al., 2020; Feng et al., 2022).

At present, the SST retrieval algorithms for microwave remote sensing include primarily physical algorithms (Meissner and Wentz, 2012; Koner and Harris, 2015; Wentz, 2000; Bettenhausen et al., 2006; Brown et al., 2006) and empirical algorithms (Goodberlet et al., 1990; Wentz, 2000; Obligis et al., 2005; Krasnopolsky et al., 2000). The multiple linear regression (MLR) algorithm, one of the empirical algorithms, can be used as an on-board SST retrieval algorithm, as it has minimal computational requirements.

We aimed to develop an on-board SST retrieval algorithm suitable for 1D-MSAMR. In this study, a new SST retrieval algorithm based on MLR, the two-step retrieval algorithm (TSSR), for 1D-MSAMR is proposed. We used the ocean-atmosphere microwave radiation brightness temperature model and the 1D-MSAMR simulator to simulate the brightness temperature detected by 1D-MSAMR. TSSR and MLR were used to retrieve SST. Ample research has demonstrated that the C-band is the most sensitive to SST and is an important frequency band for SST retrieval (Wentz and Meissner, 2007; Ai et al., 2020). In addition, Feng et al. (2022) studied the influence of different frequency combinations on SST retrieval accuracy and showed that the 5-frequency combination scheme resulted in the highest SST retrieval accuracy. Therefore, we assumed that the frequencies of the 1D-MSAMR were 6.9, 10.65, 18.7, 23.8, and 36.5 GHz and that all frequencies worked in a dual polarization (vertical and horizontal) manner. Through the simulation model, we investigated the relationship between the retrieval accuracy and the brightness temperature measurement errors EM_b of 1D-MSAMR within the incidence angle range of 0–65°.

This article is organized as follows. Section 2 introduces measured brightness temperature simulation and the SST retrieval algorithms. The results and discussion are provided in Section 3, followed by conclusions in Section 4.

2 Brightness temperature simulation and SST retrieval algorithms

2.1 Ocean-atmosphere microwave radiation brightness temperature model

We built an ocean-atmosphere microwave radiation brightness temperature model to simulate the brightness temperature received by the 1D-MSAMR ($T_{B,p,\theta}$) as follows:

$$\boldsymbol{T_{B,\,p,\theta}} = \boldsymbol{T_{BU,\theta}} + \boldsymbol{\tau_\theta} \cdot \boldsymbol{E_{p,\theta}} \cdot \boldsymbol{T_S} + \boldsymbol{\tau_\theta} \cdot \boldsymbol{T_{B\Omega,\theta}}$$

$$\boldsymbol{T_{B\Omega,\theta}} = \boldsymbol{R_{p,\theta}} \cdot \left[\boldsymbol{T_{BD,\theta}} + \boldsymbol{\tau} \cdot \boldsymbol{T_{cold}}\right] + \boldsymbol{T_{B,scat,p,\theta}}$$

$$\boldsymbol{T_{B,scat,p,\theta}} == \boldsymbol{\Omega_{p,\theta}}(\boldsymbol{\tau}, \boldsymbol{W}) \cdot \left[\boldsymbol{T_{BD,\theta}} + \boldsymbol{\tau_\theta} \cdot \boldsymbol{T_{cold}}\right] \cdot \boldsymbol{R_{p,\theta}}$$

where p denotes the polarization mode, $p = v, h$. τ_θ is the atmospheric transmittance of the entire atmosphere, $R_{p,\theta} = 1 - E_{p,\theta}$ is sea surface reflectance, and $E_{p,\theta}$ is sea surface emissivity. $T_{BU,\theta}$ is upward atmospheric radiation brightness temperature and $T_{BD,\theta}$ is downward atmospheric radiation brightness temperature. Further, T_{cold} is the effective cold space temperature, which is assumed to be a fixed value of 2.7 K, T_s is the SST, $T_{B\Omega,\theta}$ is the upward sky radiation brightness temperature scattered from the ocean surface, and $\tau \cdot T_{B,scat,p,\theta}$ is used to correct atmospheric path in the downwelling scattered sky radiation. $\Omega_{p,\theta}$ is the empirical correction parameter.

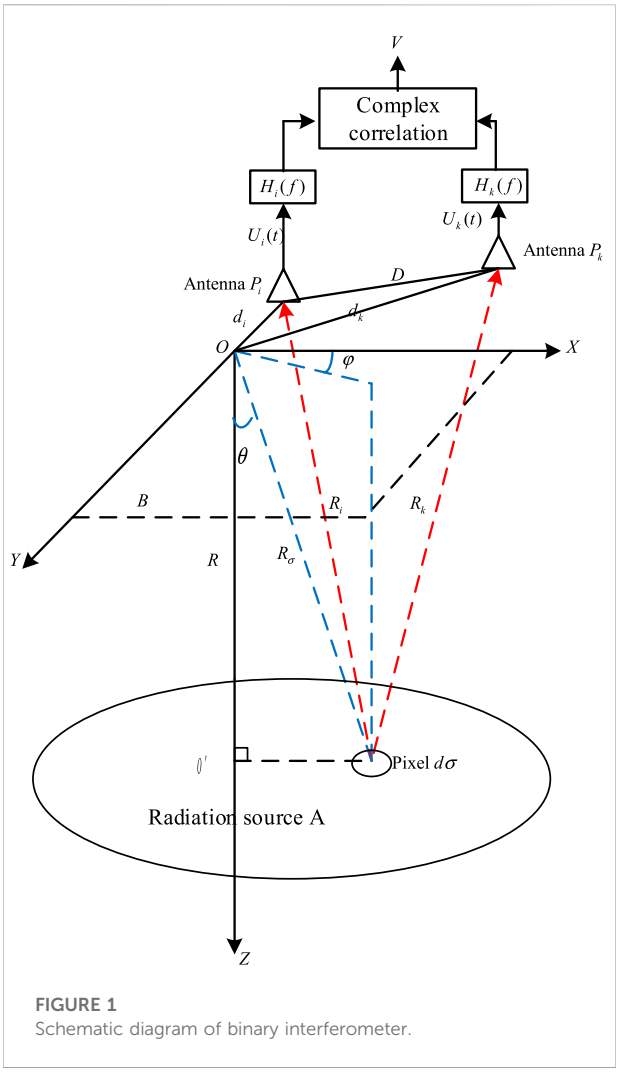

FIGURE 1
Schematic diagram of binary interferometer.

The ocean-atmosphere microwave radiation brightness temperature model is divided into two parts, the atmospheric absorption emission model, and the sea surface emissivity model. The atmospheric absorption emission model used in this study was developed by Wentz (2000) for the AMSR. The sea surface emissivity model used in this study was developed by Meissner and Wentz (2012). The model assumes that the sea surface roughness is only related to the sea surface wind vector, and the specific formula for calculation of sea surface emissivity was not provided.

2.2 The 1D-MSAMR simulator and EMb simulation

The 1D-MSAMR simulator is used to simulate the entire process of 1D-MSAMR detection of bright temperature. The schematic diagram of the detection process is shown in Figure 1.

The 1D-MSAMR uses the principle of binary interference imaging wherein P_i and P_k are two small antennas, $d\sigma$ is a pixel in the radiation source A, and source radiation is received by the small antennas at the same time. The output signals of the two small antennas are processed using complex correlation to obtain the visibility function. The visibility function is then inversely calculated to obtain the brightness temperature image of the observation scene (Schanda, 1979; Ruf et al., 1988). The output voltages are denoted by $U_i(t)$ and $U_k(t)$, where t is a limited period of time, and $H_i(f)$ and $H_k(f)$ are the frequency responses of the receiving channel. Furthermore, D is the distance of the small antenna, D_i and D_k are the distances from each small antenna to the origin o, R_i and R_k are the distances from the pixel to each small antenna, and R_σ is the distance from the pixel to o. The zenith and azimuth angles are denoted by θ and φ, respectively. After correlation calculations, it was concluded that V is only related to the distance between the two antennas (Corbella et al., 2004).

The formula for calculation of the visibility function and image reconstruction of the microwave interferometric radiometer with the 1D-MSAMR simulator is as follows (Wentz and Meissner, 2007; Lise et al., 2018):

$$V_m = \frac{1}{\sqrt{\Omega_m}} \int_{\xi^2 \le 1} \frac{T_B(\xi)}{\sqrt{1-\xi^2}} \cdot F_m(\xi) \cdot \tilde{r}_m\left(-\frac{u_m \xi}{f_c}\right) \cdot exp(-j2\pi u_m \xi) d\xi$$

$$\hat{T}(\xi) = \sum_{m=-N}^{N} V_m \, exp(j2\pi u_m \xi)$$

where Ω_m is the stereo angle of the antenna, $V_m(u_m)$ is the visibility function, $u_m = m \cdot \Delta u$ is the baseline composed of two antennas at different positions, $F_m(\xi)$ is the normalized voltage pattern, $T_B(\xi)$ is the brightness temperature of the observation scene, $\tilde{r}_m$ is the stripe elimination function, $\xi = sin\,\theta$, and f_c is the operating frequency.

We used the brightness temperature received by the 1D-MSAMR to calculate the model brightness temperature $T_{B,mod}$ with the 1D-MSAMR simulator. The antennas and channel of the 1D-MSAMR simulator used in this study were all in an ideal state, so the measured brightness temperature $T_{\theta,p}^{meas}$ was simulated by adding EM_b to the model brightness temperature $T_{B,mod}$. EM_b were assumed to follow a Gaussian distribution; in the absence of satellite observation data, it is a reasonable pre-research method used by many researchers (Bobylev et al., 2010).

2.3 SST retrieval algorithm

Figure 2 shows the schematic diagram of the SST retrieval experiment. First, we established a complete data set describing the background field of the atmosphere and ocean environment.

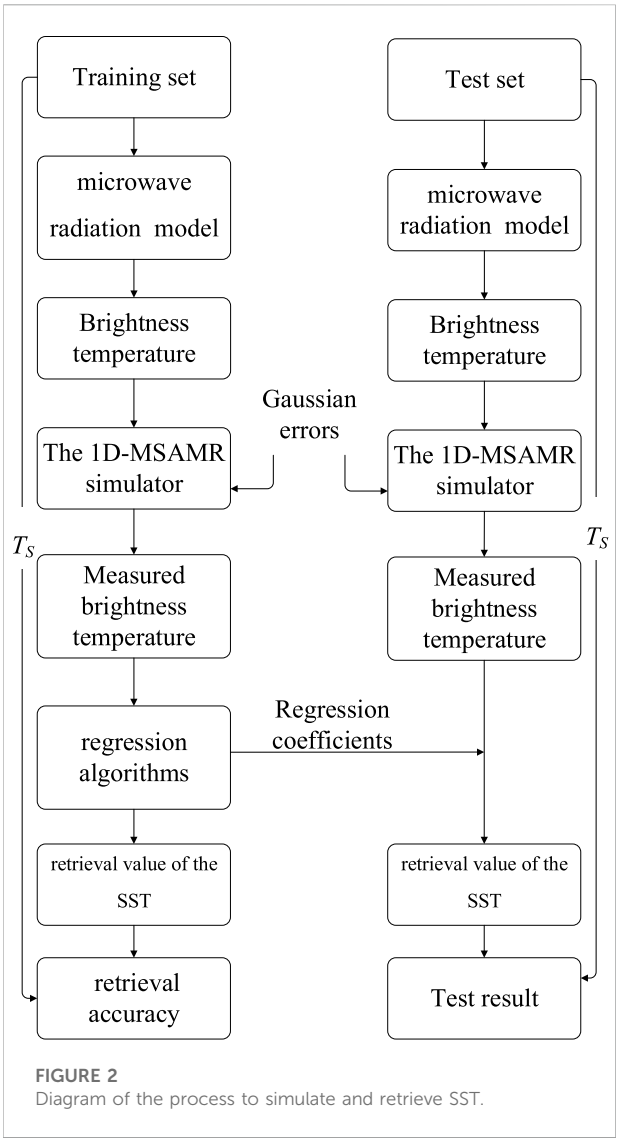

FIGURE 2
Diagram of the process to simulate and retrieve SST.

The data were then divided into training and test sets. The second step was to establish an ocean-atmosphere microwave radiation brightness temperature model to calculate the brightness temperature received by the 1D-MSAMR. The simulator with different Gaussian noises was then used to simulate the measured brightness temperature ($T_{\theta,p}^{meas}$) of the 1D-MSAMR. The last step was to establish a regression relationship between the $T_{\theta,p}^{meas}$ and SST. The obtained regression coefficient was then verified by using the test data set.

The 1D-MSAMR has the characteristics of multiple incidence angles that influence the brightness temperature considerably. Therefore, SST must be retrieved separately from different incidence angles. We used two different SST retrieval algorithms: MLR and TSSR (based on MLR). Calculation of MLR (Wentz and Meissner, 2007) was as follows:

$$T_{s,\theta} = A_{\theta,0} + \sum_{i=1}^{10\,or\,8} a_{\theta,p,i} \cdot t_{\theta,p,i}$$

$$t_{\theta,p,i} = T_{\theta,p,i}^{meas} \quad for\ 6.9,\ 10.65 GHz$$

$$t_{\theta,p,i} = -ln\left(290 - T_{\theta,p,i}^{meas}\right) \quad for\ 18.7,\ 23.8,\ 36.5\ GHz$$

where $A_{\theta,0}$ is a constant term, $a_{\theta,p,i}$ is the regression coefficient, and the subscript i corresponds to different frequencies.

For TSSR, $T_{\theta,p}^{meas}$ and MLR were used first to retrieve the preliminary SST retrieval value ($T_{S,first}$), which was then used as "*a priori*" in a second step to divide $T_{\theta,p}^{meas}$ data. $T_{\theta,p}^{meas}$ data were divided into different data sets in accordance with $T_{S,first}$ for 2 K intervals within 273.15 K–313.15 K. Then we trained the divided data sets to obtain the regression coefficients of each set using MLR. The last step was to use the regression coefficients to retrieve SST ($T_S^{retrieval}$). In the retrieval process, the training set was used to calculate the regression coefficients, and the test set was used to verify the regression coefficients. The specific process is shown in Figure 3.

3 Results and discussion

3.1 Data

This study used the data products of WindSat in Remote Sensing Systems (RSS) to establish the background field data. The data were 7-day average data product worldwide from 2016 to 2018. Specifically, the data included SST (T_s), total atmospheric column water vapor content (V), total atmospheric column cloud liquid water content (L), rainfall rate (R), wind direction at 10 m height (φ), and wind speed at 10 m height (W).

This research focused on the retrieval of SST in the case of non-precipitation; therefore, we excluded data with $R > 0mm/h$. We further excluded data corresponding to $V > 50mm$ and $L > 0.2mm$ due to the limitations of the ocean-atmosphere microwave radiation brightness temperature model. The remaining data contain about 2.1 million sets of data. Our data is randomly divided into training and test sets. Figure 4 shows data histograms. Since seawater salinity is more sensitive to the L-band (1.4 GHz) and has little influence on the frequencies used in this study, we also set the seawater salinity to the value of 35 psu (Feng et al., 2021.).

3.2 Results and discussion

We used the root mean square error (RMSE) to represent the retrieval error:

$$\sigma = \sqrt{\frac{1}{N}\sum_{k=1}^{N}\left(T_{S,k}^{true} - T_{S,k}^{retrieval}\right)^2}$$

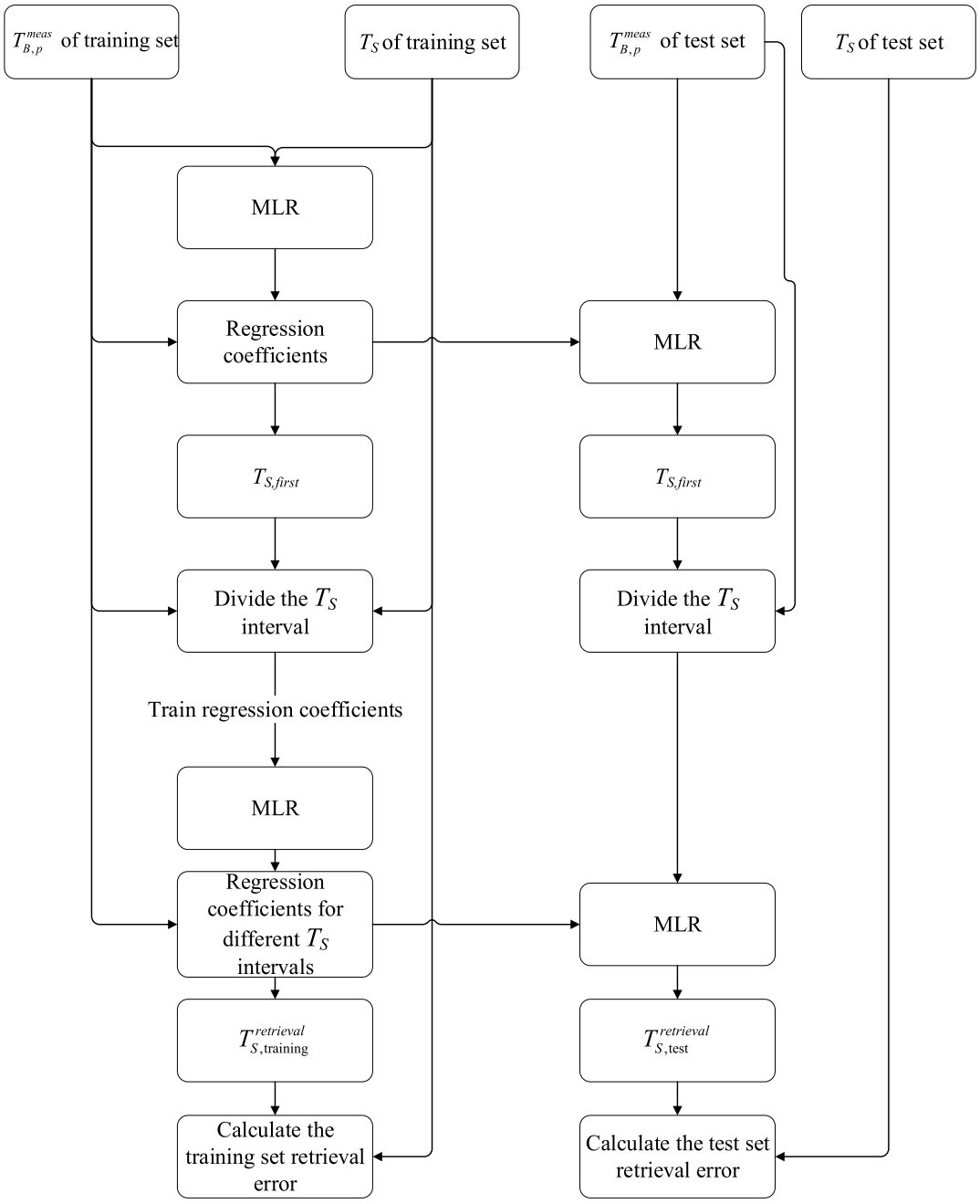

FIGURE 3
Flow chart of two-step algorithms.

where σ represents the RMSE, $T_{S,k}^{true}$ is the true value of the SST, $T_{S,k}^{retrieval}$ denotes the retrieval value of the SST, and N represents the number of $T_{S,k}^{true}$.

Figure 5 shows the relationship between the SST retrieval errors and the incidence angle when all channels of the 1D-MSAMR have the same EM_b (a massif of random Gaussian distribution with a zero mean and σ = 0~1 K). The figure demonstrates that the SST retrieval errors of the training set and the test set were almost the same for the two SST retrieval algorithms. This shows that the two SST retrieval algorithms are generalizable. In addition, the SST retrieval errors of TSSR were less than MLR, especially at low incidence angle and large EM_b. When EM_b of each channel of the 1D-MSAMR was within the range of 0~1 K, the SST retrieval error ranges of the test set and

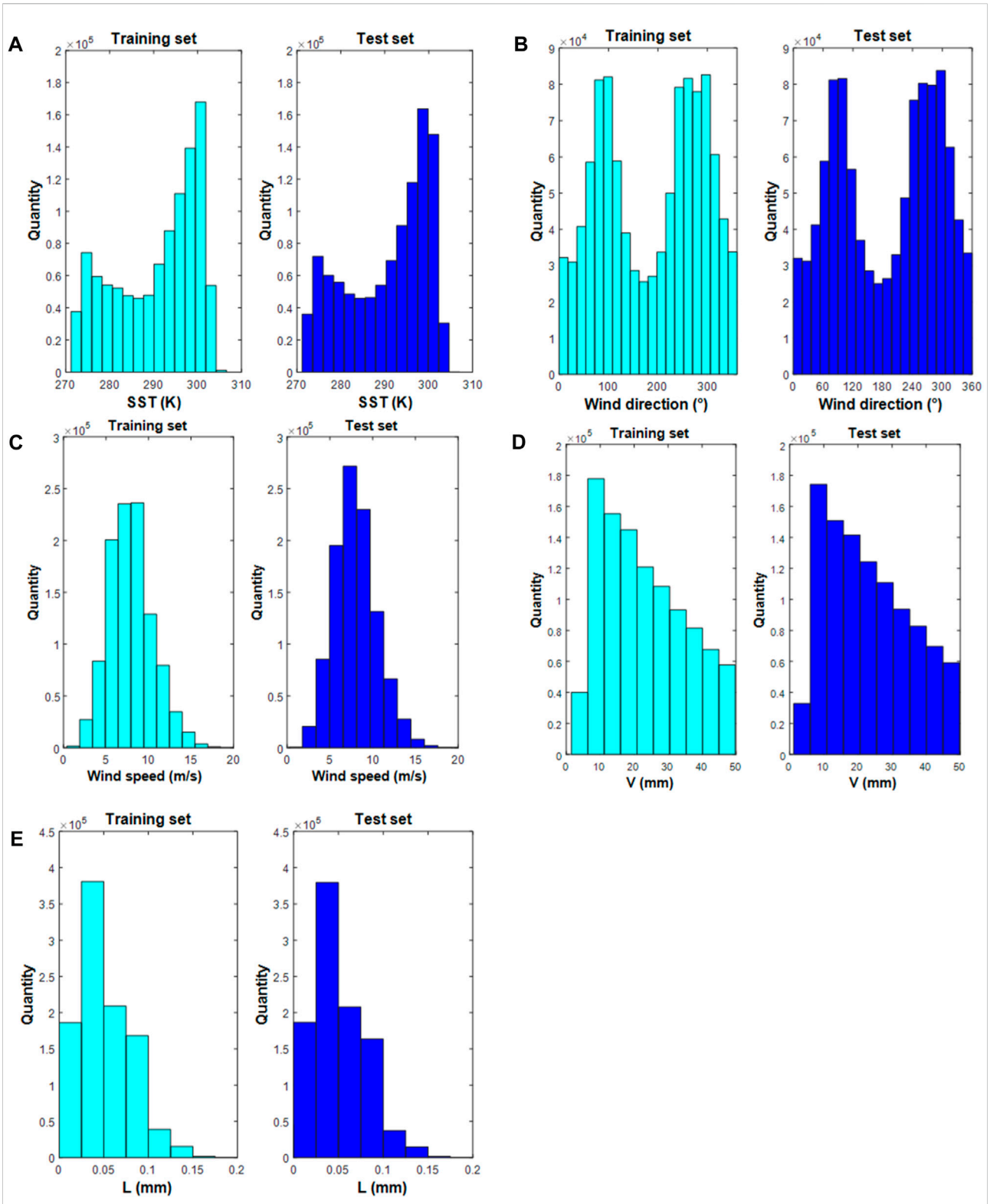

FIGURE 4
Histograms of the atmospheric-ocean background field data. The training set is shown on the left and the test set on the right. **(A)** SST; **(B)** sea surface wind direction; **(C)** sea surface wind speed; **(D)** water vapor content; and **(E)** liquid water content.

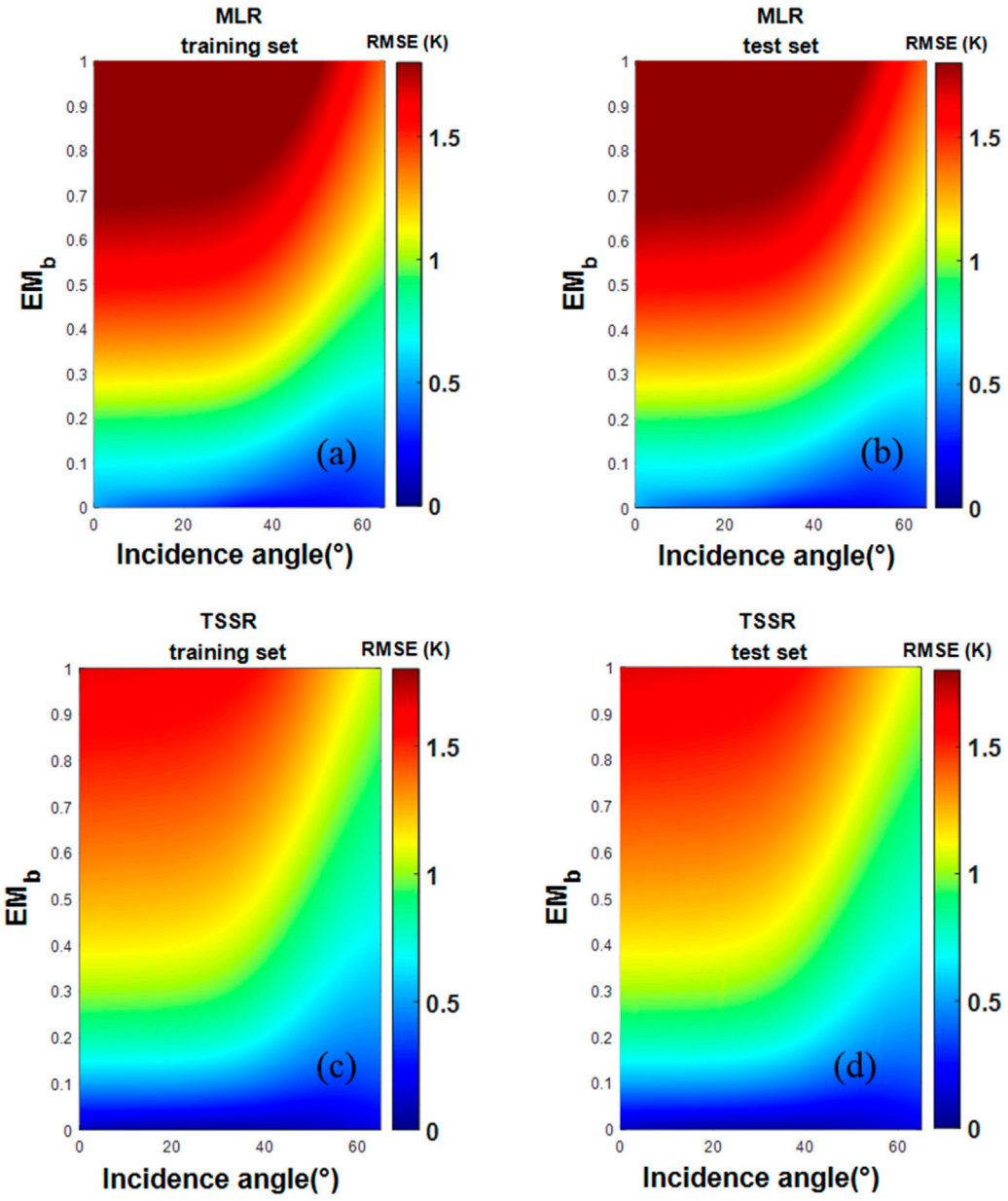

FIGURE 5
Relationship between SST retrieval errors, incidence angle, and EM_b. **(A,B)** MLR train and test; **(C,D)** TSSR train and test.

training set for MLR were 0.21 K–2.14 K and 0.21 K–2.15 K, respectively, and the retrieval error ranges of TSSR were 0.04 K–1.67 K and 0.04 K–1.66 K, respectively. The Gaussian error added by each channel was generated separately.

Figure 6 further illustrates the SST retrieval errors *versus* the incidence angle in the case of different EM_b. The SST retrieval errors of TSSR and MLR decreased with increasing incidence angle. This suggests that larger incidence angles should be set for the 1D-MSAMR to improve SST retrieval accuracy. Feng et al. (2022). reached a similar conclusion when analyzing the influence of frequency combination on the retrieval accuracy of SST and pointed out that an incidence angle set between 30°–60° is most conducive to the retrieval of SST. For different EM_b, the SST retrieval errors of test sets are provided in Table 1. These data indicate that the SST retrieval accuracy decreased with increasing EM_b and the average SST retrieval accuracy of TSSR was about 0.3 K (25%) higher than that of MLR. These results suggest that the 1D-MSAMR system error should be reduced as much as possible with redesign of its hardware system.

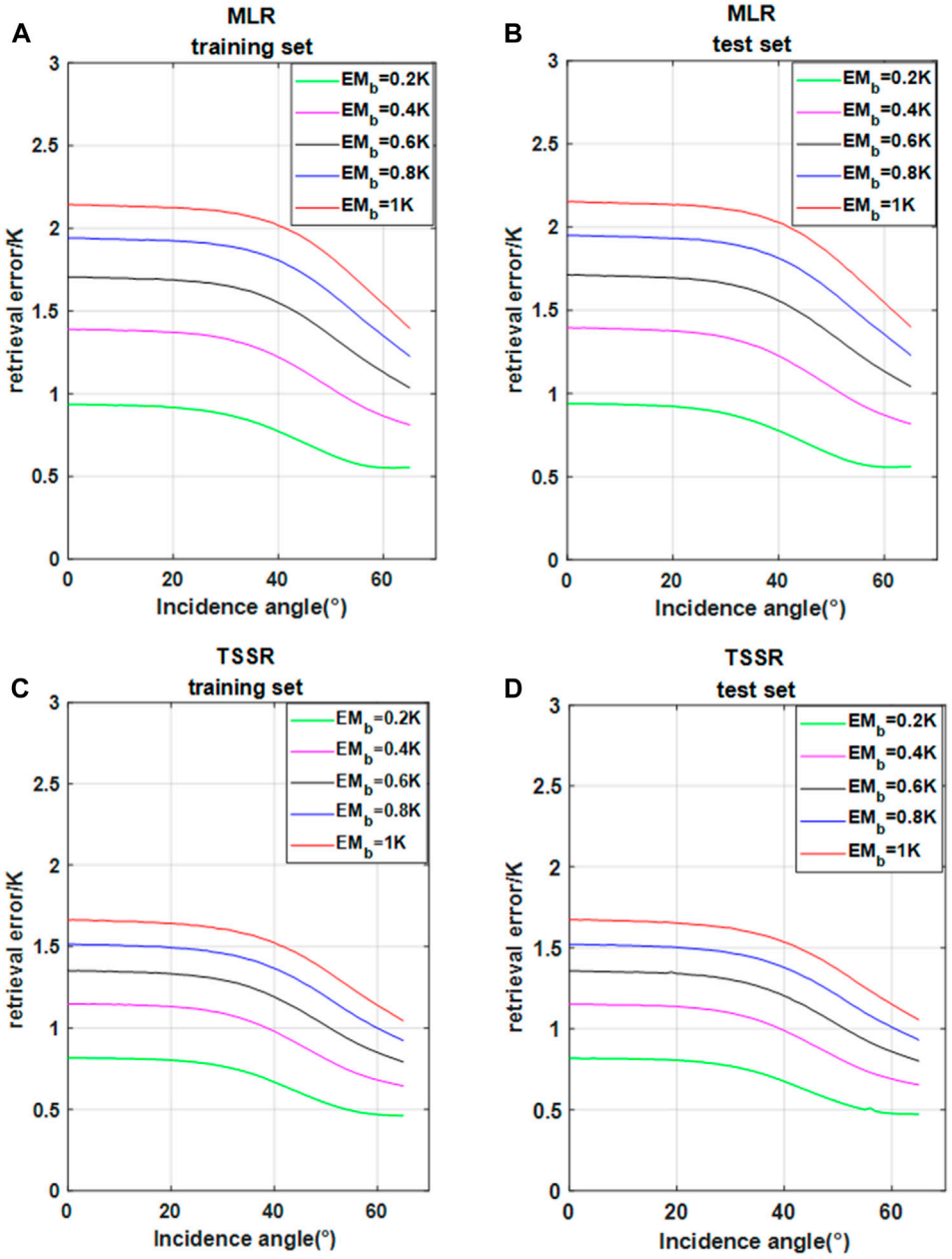

FIGURE 6
Relationship between SST retrieval error and incidence angle for different EM_b. **(A,B)** MLR train and test; **(C,D)** TSSR train and test.

C-band is the band that is most sensitive to SST. Sensitivity to the 6.9 GHz frequency (C_{sens}) is proposed to quantitatively describe the relationship between the EM_b of 6.9 GHz and SST retrieval accuracy. C_{sens} is calculated as follows:

$$C_{sens} = \frac{\partial \sigma}{\partial EM_b}$$

where σ is the RMSE of retrieval error and EM_b is brightness temperature measurement error.

The relationship between C_{sens} of the two SST retrieval algorithms and the EM_b is given in Figure 7. The C_{sens} decreased rapidly with increasing EM_b. This shows that with the increasing EM_b of 6.9 GHz, the C_{sens} curve decreases rapidly and finally trends to zero, which indicates that the retrieval accuracy of SST decreases rapidly when there is a measurement error in the 6.9 GHz channel. However, when the measurement error is greater than a certain value, the retrieval accuracy of SST remains stable. The C_{sens} curve

TABLE 1 SST retrieved with different dilation values.

EM_b (K)	Retrieval accuracy of TSSR (K)	Retrieval accuracy of MLR (K)
0	0.04–0.15	0.21–0.53
0.1	0.33–0.51	0.39–0.69
0.2	0.47–0.82	0.56–0.94
0.3	0.57–1.02	0.69–1.19
0.4	0.65–1.15	0.81–1.40
0.5	0.73–1.26	0.93–1.57
0.6	0.80–1.36	1.04–1.71
0.7	0.87–1.44	1.14–1.84
0.8	0.93–1.52	1.23–1.95
0.9	0.99–1.60	1.32–2.05
1	1.06–1.67	1.40–2.15

(black line) corresponding to TSSR is always below the MLR curve (red line), which shows that the TSSR is less affected by the EM_b of 6.9 GHz. That is, TSSR can reduce the negative impact of 6.9 GHz channel measurement error on the retrieval accuracy of SST, and with an increase in 6.9 GHz channel measurement error, the retrieval accuracy of SST will regain stability faster.

Among future on-board sensors for remote sensing of SST, 1D-MSAMR has excellent potential. This study used the MLR algorithm, which has fast computation speed and small computational memory requirements, to develop an on-board SST retrieval algorithm for 1D-MSAMR. Although the systematic error terms of each channel of 1D-MSAMR cannot be accurately obtained, the maximum error was set at the upper limit of 1 K according to the systematic error published by the on-orbit real-aperture microwave radiometer. Surprisingly, TSSR improved the retrieval accuracy by about 25% on the basis of only one more set of regression coefficients compared to MLR, and TSSR was less affected by the EMb of 6.9 GHz. Therefore, the requirement of 6.9 GHz channel design can be appropriately reduced when TSSR is adopted. One reason for the improved performance of TSSR *versus* MLR is that, with TSSR, the initial retrieval value of SST is divided into intervals and then each interval is retrieved separately. The SST has obvious zonal distribution characteristics (high SST at low latitude), and the sensitivity of each channel to SST is nonlinear (Feng et al., 2021). Therefore, it is more reasonable to adopt different coefficients for different SSTs. TSSR has the capacity for automatic operation without manual intervention. After running for a period of time, the algorithm can automatically update the coefficients of the two-step method and improve the retrieval accuracy by using the temperature data of the sea buoy. However, this study was based on simulation data. Although the Gaussian error we added to each channel was generated separately, the error of each channel has the same distribution (mean value is 0, variance is the same), which is not common in the actual 1D-MSAMR system. Although our simulation model is scientific, it still needs future verification and adjustment based on actual 1D-MSAMR measurement data.

Due to the different baselines of small antennas at different frequencies, it is difficult for the spatiotemporal synchronous observation areas to coincide completely, which leads to the problem of high spatial resolution at high frequencies and low spatial resolution at low frequencies. However, the premise of TSSR algorithm application is that the measured brightness temperature of each channel has spatiotemporal matching. Therefore, before applying TSSR, it is necessary to preprocess the measured brightness temperature so that the measured brightness temperature of each channel corresponds to the same detection area.

There is an advantage to using a microwave radiometer to monitor SST under conditions of weak precipitation. Precipitation will increase the roughness and change the emissivity of the sea surface. Due to limitations of the simulation model, the sea surface emissivity in the presence of precipitation cannot be calculated, so we did not study the retrieval of SST under those conditions; future studies will address measurement of SST *via* the 1D-MSAMR in the presence of precipitation. The 1D-MSAMR used in our study has five frequencies. The detected brightness temperature contains more information about the sea surface and atmospheric environment, and the five frequencies include those that are sensitive to water vapor content and weak precipitation (23.8 GHz and 36.5 GHz, respectively). Therefore, 1D-MSAMR retrieval of SST under conditions of weak precipitation is theoretically feasible, and a direction to be explored in our future research.

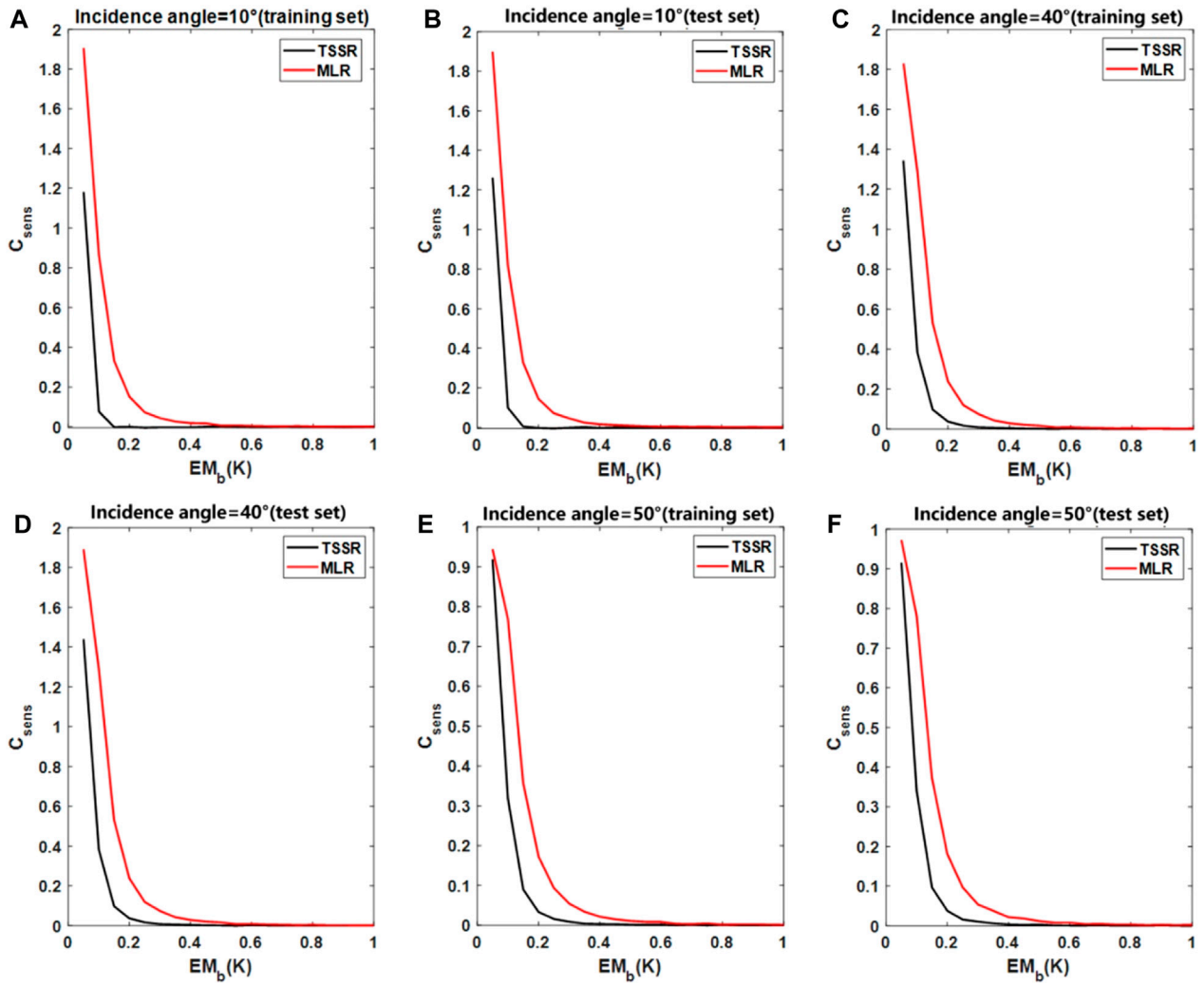

FIGURE 7
Relationship between C_{sens} and EM_b for different antenna angles. **(A,B)** the incidence is 10°, **(C,D)** the incidence is 40°, **(E,F)** the incidence is 60°.

4 Conclusion

MLR requires minimal computation capacity, which makes it a good option for an on-board retrieval algorithm. In this study, an SST retrieval algorithm (TSSR) was proposed to evaluate the SST retrieval error for 1D-MSAMR based on MLR. We investigated the relationship between retrieval errors and brightness temperature measurement errors (EM_b) of the 1D-MSAMR within the incidence angle range of 0–65°. Sensitivity of the SST retrieval algorithms to the 6.9 GHz frequency (C_{sens}) was also assessed. TSSR has higher retrieval accuracy than the MLR algorithm, especially at low incidence angle. The average retrieval accuracy of the TSSR was about 0.3 K higher than that of the MLR algorithm. Moreover, the two-step algorithm had less sensitivity to EM_b of the 6.9 GHz frequency. In summary, TSSR can be used as an on-board retrieval algorithm for 1D-MSAMR. In the design of 1D-MSAMR, the incidence angles should be in as large a range as possible, and the system errors should be reduced as much as possible.

Data availability statement

The original contributions presented in the study are included in the article/Supplementary Material; further inquiries can be directed to the corresponding author.

Author contributions

Conceptualization, CG and WA; methodology, CG and WA; software, SH and MF; validation, JQ, WA, and SH; formal analysis, JQ and WA; investigation, JQ and WA; resources, SH;

data curation, JQ and WA; writing—original draft preparation, JQ and WA; writing—review and editing, JQ and WA; visualization, JQ and WA; supervision, ML; project administration, JQ and WA.

Acknowledgments

We would like to express our gratitude to Professor Frank J. Wentz for his great help in our research. We are thankful for the support from the National Natural Science Foundation of China (41605016). We would like to express our gratitude to Edit Springs (https://www.editsprings.com/) for the expert linguistic services provided. We acknowledge WindSat in Remote Sensing Systems (RSS) for providing the data. The data, including the RSS WindSat Data Products, can be obtained online (http://www.remss.com/missions/windsat/).

Conflict of interest

The authors declare that the research was conducted in the absence of any commercial or financial relationships that could be construed as a potential conflict of interest.

Publisher's note

References

Ai, W., Feng, M., Chen, G., and Lu, W. (2020). Research on sea surface temperature retrieval by the one-dimensional synthetic aperture microwave radiometer, 1D-SAMR. *Acta Oceanol. Sin.* 39 (5), 115–122. doi:10.1007/s13131-020-1540-1

Bobylev, L. P., Leonid, E., ZabolotskikhElizaveta, V., Mitnikand Leonid, M. (2010). Atmospheric water vapor and cloud liquid water retrieval over the arctic ocean using satellite passive microwave sensing. *IEEE Trans. Geosci. Remote Sens.* 48, 283–294. doi:10.1109/TGRS.2009.2028018

Bettenhausen, M. H., Smith, C.K., Bevilacqua, R. M., Wang, N. Y., Gaiser, P. W., and Cox, S.(2006). A nonlinear optimization algorithm for WindSat wind-vector retrievals. *IEEE Trans. Geosci. Remote Sens.* 44(3), 597–610. doi:10.1109/tgrs.2005.862504

Brown, J., Simmonds, I., and Noone, D.(2006). Modeling delta O-18 in tropical precipitation and the surface ocean for present-day climate. *Journal of Geophysical Research-Atmospheres*. 111(D5). doi:10.1029/2004jd005611

Chelton, D. B., and Wentz, F. J. (2005). Global microwave satellite observations of sea surface temperature for numerical weather prediction and climate research. *Bull. Am. Meteorol. Soc.* 86 (8), 1097–1116. doi:10.1175/BAMS-86-8-1097

Corbella, I., Duffo, N., Vall-llossera, M., Camps, A., and Torres, F. (2004). The visibility function in interferometric aperture synthesis radiometry. *IEEE Trans. Geosci. Remote Sens.* 42 (8), 1677–1682. doi:10.1109/TGRS.2004.830641

Feng, M., Ai, W., Chen, G., Lu, W., and Ma, S. (2022). A multiple linear regression algorithm for sea surface temperature retrieval by one-dimensional synthetic aperture microwave radiometry. *J. Atmos. Ocean. Technol.* 37 (9), 1753–1761. doi:10.1175/JTECH-D-20-0003.1

Feng, M., Ai, W., Lu, W., Shan, C., Ma, S., and Chen, G. (2021). Sea surface temperature retrieval based on simulated microwave polarimetric measurements of a one-dimensional synthetic aperture microwave radiometer. *Acta Oceanol. Sin.* 40 (3), 122–133. doi:10.1007/s13131-021-1712-7

Goodberlet, M. A., Swift, C. T., and Wilkerson, J. C. (1990). Ocean surface wind speed measurements of the Special Sensor Microwave/Imager (SSM/I). *IEEE Trans. Geosci. Remote Sens.* 28 (5), 823–828. doi:10.1109/36.58969

Jin, R., Li, Q., and Liu, H. (2019). A subspace algorithm to mitigate energy unknown RFI for synthetic aperture interferometric radiometer. *IEEE Trans. Geosci. Remote Sens.* 58 (99), 227–237. doi:10.1109/TGRS.2019.2936005

Jordi, F., Camps, A., Andres, B., Martin-Neira, M., Boutin, J., Reul, N., et al. (2010). Smos: The challenging sea surface salinity measurement from space. *Proc. IEEE* 98 (5), 649–665. doi:10.1109/JPROC.2009.2033096

Koner, P. K., and Harris, A.(2015). " A deterministic inversion technique for sea surface temperature retrieval from MODIS radiances," in Conference on Ocean Sensing and Monitoring VII. doi:10.1117/12.2179868

Krasnopolsky, V. M., Gemmill, W. H., and Breaker, L. C.(2000). A neural network multiparameter algorithm for SSM/I ocean retrievals: Comparisons and validations. *Remote Sens. Environ.* 73 (2), 133–142. doi:10.1016/s0034-4257(00)00088-2

Lambrigtsen, B., Brown, S., Gaier, T., Kangaslahti, P., Tanner, A., and Wilson, W. (2006). "GeoSTAR : Developing a new payload for GOES satellites," in Aerospace Conference (IEEE).Big Sky, MT, March October 04–11, 2006

Le, V., and David, M. (1990). The sensitivity of synthetic aperture radiometers for remote sensing applications from space. *Radio Sci.* 25 (4), 441–453. doi:10.1029/rs025i004p00441

Le, V., Griffis, A., J., Swift, C., T., and Jackson, T. (1994). Estar: A synthetic aperture microwave radiometer for remote sensing applications. *Proc. IEEE* 82 (12), 1787–1801. doi:10.1109/5.338071

Li, Q., Ke, C., Wei, G., Liang, L., and Chen, L. (2008). "An aperture synthesis radiometer at millimeter wave band," in International Conference on Microwave & Millimeter Wave Technology, Nanjing, 21-24 April 2008.

Lise, K., Catherine, P., Filipe, A., Boutin, J., Heygster, G., Tonboe, R. T., et al. (2018). Expected performances of the copernicus imaging microwave radiometer (CIMR) for an all-weather and high spatial resolution estimation of ocean and sea ice parameters. *J. Geophys. Res. Oceans* 123 (110), 7564–7580. doi:10.1029/2018JC014408

Meissner, T., and Wentz, F. J. (2012). The emissivity of the ocean surface between 6 and 90 GHz over a large range of wind speeds and earth incidence angles. *IEEE Trans. Geosci. Remote Sens.* 50 (8), 3004–3026. doi:10.1109/TGRS.2011.2179662

Obligis, E., Labroue, S., Amar, A., Thiria, S., Crepon, M., and Mejia, C.(2005). RETRIEVING THE OCEAN SALINITY FROM SMOS OBSERVATIONS BY THE USE OF NEURAL NETWORKS.

Prigent, C., Aires, F., Bernardo, F., Orlhac, J. C., Goutoule, J. M., Roquet, H., et al. (2013). Analysis of the potential and limitations of microwave radiometry for the retrieval of sea surface temperature: Definition of MICROWAT, a new mission concept. *J. Geophys. Res. Oceans* 118 (6), 3074–3086. doi:10.1002/jgrc.20222

Ruf, C. S., Swift, C. T., Tanner, A. B., and Le Vine, D. M. (1988). Interferometric synthetic aperture microwave radiometry for the remote sensing of the Earth. *IEEE Trans. Geosci. Remote Sens.* 26 (5), 597–611. doi:10.1109/36.7685

RYLE (1962). The new cambridge radio telescope. *Nature* 194 (4828), 517–518. doi:10.1038/194517a0

Schanda, E. (1979). "Multiple wavelength aperture synthesis for passive sensing of the Earth's surface," in Antennas & Propagation Society International Symposium, Seattle, WA, USA, 18-22 June 1979, 597–611.

Ulaby, B., Moore, R. K., and Fung, A. K. (1981). Microwave remote sensing: Active and passive. Volume 1 - Microwave remote sensing fundamentals and radiometry.

Vine, D., Griffis, A., Swift, C. T., and Jackson, T. J. (1992). "Estar: A synthetic aperture microwave radiometer for measuring soil moisture," in International Geoscience & Remote Sensing Symposium. Houston, TX, May 26–29, 1992

Vine, D., Haken, M., and Swift, C. T. (2004). "Development of the synthetic aperture radiometer ESTAR and the next generation," in Geoscience and Remote Sensing Symposium, 2004. IGARSS '04. Proceedings (IEEE). Anchorage, AK, September 20–24, 2004

Vine, D. (2000). Synthetic aperture radiometer systems. *IEEE Trans. Microw. Theory Tech.* 47 (12), 2228–2236. doi:10.1109/22.808964

Wentz, F. J. (2000). Algorithm theoretical basis document (ATBD) AMSR ocean algorithm. EOS Project, Goddard Space Flight Center, National Aeronautics and Space Administration.

Wentz, F. J., and Meissner, T. (2007). Supplement 1: Algorithm theoretical basis document for AMSR-E ocean algorithms. Santa Rosa, CA: NASA.

Zine, S., Boutin, J., Font, J., Reul, N., Waldteufel, P., Gabarro, C., et al. (2008). Overview of the SMOS sea surface salinity prototype processor. *IEEE Trans. Geosci. Remote Sens.* 46 (3), 621–645. doi:10.1109/tgrs.2008.915543